Predicting novel *E. glacialis* foraging habitat for future climate scenarios on the Northeast Atlantic shelf

Omi Johnson[1, 2], Camille Ross[1], Caroline Lehoux[3], Tarik Gouhier[4], Ben Tupper[1], Chris Orphanides[5], Stéphane Plourde[3], Nicholas Record[1]

1. Bigelow Laboratory for Ocean Sciences, East Boothbay, ME, USA.
2. Khoury College of Computer Science, Northeastern University, Boston, MA, USA.
3. Fisheries and Oceans Canada, Institut Maurice-Lamontagne, Mont-joi, Québec, Canada.
4. Marine Science Center, Northeastern University, Nahant, MA, USA.
5. NOAA National Marine Fisheries Service, Northeast Fisheries Science Center, Narragansett, Rhode Island, USA.

Abstract

The critically endangered North Atlantic right whale *(Eubalaena glacialis)* faces significant anthropogenic mortalities and has been the focus of a variety of conservation efforts and legal battles. Recent climate shifts in the Gulf Stream have caused unpredictability in right whale distributions and created challenges for traditional management techniques. Early warnings of emerging *E. glacialis* habitat can help with proactive management and potentially avoid significant mortality events. *E. glacialis* primarily feeds on aggregations of *Calanus* spp. dense enough to meet bioenergetic requirements. Predicting distributions of *Calanus* spp. feeding habitats during future climate scenarios will reveal insight into future *E. glacialis* distribution shifts. In this study, we trained boosted regression tree modeling algorithms with *C. finmarchicus* and *C. hyperboreus* feeding habitat data and monthly environmental covariates to build species-specific models of present and future habitat distributions on the northeast American shelf between the Mid-Atlantic Bight and Labrador Shelf. Present-day feeding habitat data was derived by comparing species abundance data from U.S. and Canadian shelf areas to a depth-varying critical bioenergetic threshold for *E. glacialis*. Environmental covariates were sourced from fine-resolution, modeled projections of the North Atlantic and included monthly measurements of bathymetry, mixed layer depth, sea surface temperature and salinity, bottom water temperature and salinity, and current velocity. The trained models were then projected to the years 2055 and 2075 for representative concentration pathway (RCP) 4.5 and 8.5 management scenarios to examine new and lost feeding habitats relative to present day. The models had generally high performance (AUC > .9) and indicated bottom temperature and mixed layer depth as important covariates. Present-day projections correlated to known areas of high habitat suitability, as well as additional areas on the Labrador Shelf and Flemish Cap. Future projections indicated decreased habitat suitability in the Gulf of Maine and areas in the Gulf of Saint Lawrence, with retained and increased suitability in the Scotian Shelf, Newfoundland and Labrador Shelves, and the Flemish Cap. Directing some survey efforts towards emerging foraging habitats can enable conservation management to anticipate distribution shifts that have led to high mortality in the past.

1. Introduction

The North Atlantic right whale (*Eubalaena glacialis)* is one of the most critically endangered whale species on Earth, with less than 350 individuals estimated to remain (listed as 'Critically Endangered' on the IUCN redlist, Cooke 2020). *E. glacialis* populations were the target of intensive commercial whaling from the 12th through 18th centuries until the practice was banned in 1935. The population was as low as 295 individuals in 1992 (Knowlton et al. 1994), but grew steadily at a rate of 2.8% per year to reach a peak of 481 individuals in 2011 (Waring et al. 2016; Pettis et al. 2021). However, from 2010 to 2020, populations have decreased, with lowered sightings in historical feeding habitats (Pettis et al. 2021). Vessel collisions and fishing gear entanglements are significant sources of mortality for present-day populations: 85% of deaths between 2010 and 2016 are attributed to entanglement (Pettis et al. 2018; Kraus et al. 2016). Calving rates have also declined by 40% from 2010 to 2016, putting the species at risk of extinction (Kraus et al. 2016). *E. glacialis* population loss has ecological ramifications because it and other large whales serve crucial roles in replenishing nitrogen to surface waters and creating rich whale fall ecosystems (Smith and Baco 2003; Roman and McCarthy 2010). Conservation efforts to mitigate anthropogenic *E. glacialis* mortalities have been implemented for decades with varying degrees of success. Policies enacted between 1998 and 2009, such as the Atlantic Large Whale Take Reduction Plan (ALWTRP) which modified fishing equipment, did not significantly affect mortality rates (Van Der Hoop et al. 2013; Pace et al. 2014). However, more recent tactics such as lowering vessel speeds in seasonal habitats along the U.S. East Coast seem to have reduced mortality (Laist et al. 2014).

E. glacialis inhabit the east coast of North America between Florida and Newfoundland (Winn et al. 1986; Kraus and Rolland 2007). Calving occurs during the winter months near Florida and Georgia while feeding has historically occurred in Cape Cod Bay during winter and from June to September in the Gulf of Maine, Bay of Fundy, and Scotian Shelf (Kraus and Rolland 2007). The Gulf of Maine is a unique ecosystem that is also experiencing one of the fastest rates of warming in the global ocean (Pershing et al. 2015). Past management of *E. glacialis* has assumed the species would be resistant to climate change (Record et al. 2019). However, the decrease in population size and shift from traditional feeding habitats in 2010 coincides with climatic changes in the Gulf Stream which impacted bottom water temperatures in the Gulf of Maine (Record et al. 2019; Pettis et al. 2021; Neto et al. 2021). This suggests that the species is vulnerable to the effects of climate change. Shifts in the distribution of *E. glacialis* decrease the effectiveness of current conversation strategies relying on historical feeding habitats, therefore increasing the risk of anthropogenic mortality (Kraus et al. 2016). *E. glacialis* distributions prior to commercial whaling ranged across the North Atlantic, and as the climate shifts, new feeding habitats will probably emerge that could challenge management tactics. Since effective *E. glacialis* surveys are technically and logistically intensive, additional habitat identification methods will be useful to support survey area selection in regions like the Gulf of Maine experiencing rapid climate change.

E. glacialis distributions are correlated to the prey species *Calanus finmarchicus*, a lipid-rich copepod fundamental to the Northwest Atlantic ecosystem (Wisher et al. 1988;

Murison and Gaskin 1989; Mayo and Marx 1990; Baumgartner and Mate 2003; Pershing et al. 2009; Record et al. 2019; Pershing and Stamieskin 2020). *C. finmarchicus* is an energy-rich prey source for *E. glacialis* because it aggregates dense amounts of lipids during diapause (Ji 2011). *C. finmarchicus* has traditionally occupied regions from the Irminger and Labrador seas near Greenland to the northern edge of the Mid-Atlantic Bight (Conover 1988); however, the preferred depth and temperature requirements of diapause make *C. finmarchicus* especially vulnerable to climate change (Wilson et al. 2016). Other arctic *Calanus* species such as *Calanus hyperboreus* and *Calanus glacialis* are also potentially suitable prey species for *E. glacialis* (Lehoux et al. 2020). These species currently inhabit waters from the Scotian Shelf northward (Head and Pepin 2010), and may become increasingly important if *E. glacialis* distributions continue to move to higher latitudes (Davis et al. 2017; Plourde et. al. 2019; Davis et al. 2020; Meyer-Gutbrod et al. 2021; Meyer-Gutbrod et al. 2022). *E. glacialis* appear to select foraging areas where *Calanus* spp. abundances are above a critical threshold satisfying bioenergetic requirements (Mayo and Marx 1990, Kenney and Wishner 1995, Plourde et. al. 2019). Considering current distributions of *Calanus* spp. aggregations and how they may shift with climate change will reveal insight into preferred *E. glacialis* foraging habitats.

Species distribution models (SDMs) use environmental covariates to predict species abundance and can be an effective tool to identify areas of habitat suitability (Elith et. al. 2006). A variety of past models have been developed to examine present and future distributions of *Calanus* spp. (e.g., Reygondeau and Beaugrand 2011; Ji 2011**;** Chust et al. 2014; Villarino et al. 2015; Grieve et al. 2017). However, few have focused on *Calanus* spp. abundance relative to the bioenergetic needs of *E. Glacialis* (e.g., Pendleton et al. 2012; Plourde et al. 2019; Ross et al. in press). Additionally, many only consider the U.S. or Canadian regions of the contiguous northeast continental shelf or do not have sufficiently high resolution to accurately model the complex currents around the Gulf of Maine (Brickman et. al. 2021). By considering multiple prey species, merging abundance data from both U.S. and Canadian waters, and using high-resolution future projections of environmental covariates, we can provide detailed, comprehensive projections of current and future *E. Glacialis* feeding grounds over the entire domain of this highly migratory species, which no study has attempted previously.

To examine how *E. glacialis* habitats may shift due to climate change, we built SDMs to predict *E. glacialis* feeding habitat suitability based on *Calanus* spp. abundance. We developed dynamic *Calanus* spp. density thresholds for suitable feeding habitats based on estimated bioenergetic needs for *E. glacialis*. The thresholds were separately applied to *C. finmarchicus* and *C. hyperboreus* abundance data from the Gulf of Maine, Scotian Shelf, Gulf of Saint Lawrence, and Newfoundland and Labrador Shelves to identify suitable and unsuitable present-day feeding areas. *C. glacialis* was omitted from this study because there was insufficient high-abundance data to enable reliable modeling. We then built boosted regression tree SDMs using the derived suitability data and high-resolution covariates from Brickman et al. (2021). Boosted regression trees are ensemble, tree-based models chosen for their high performance and capability to learn data in detail (Elith et al. 2008). Potential feeding habitats were projected by coordinates, month, and prey species to 2055 and 2075 under the Intergovernmental Panel on Climate Change (IPCC) representative concentration pathway

(RCP) 4.5 and 8.5 scenarios. The prey-specific projections were also combined to create comprehensive, multi-species predictions of new and lost *E. glacialis* feeding habitats over its entire domain. The resulting habitat maps can be used to examine shifts in *E. glacialis* feeding grounds and inform new target areas for survey or conservation efforts.

2. Methods

2.1. Study Area

The study extent covered the Gulf of Maine (GoM), Scotian Shelf (SS), Gulf of Saint Lawrence (GSL), and Newfoundland and Labrador Shelves (NLS) between 36.5° to 56.7°N and -77.0° to -42.5°W (Figure 1). This domain includes the entire extent of the contributing *Calanus* spp. datasets as well as historically important *E. Glacialis* feeding habitats such as Cape Cod Bay, the Great South Channel, the Bay of Fundy, and the Roseway Basin (Ross et al. 2021). The domain also includes areas potentially suitable for future *E. Glacialis* foraging habitats such as the SS and GSL (Plourde et al. 2019; Meyer-Gutbrod et al. 2022).

2.2. Environmental covariate data

Environmental covariates were sourced from the high-resolution climate model created by Brickman et al. (2016) (hereby referred to as the “Brickman datasets”). The Brickman datasets were generated by applying downscaling techniques to force high-resolution (1/12°) ocean models of the Northern Atlantic. Present-day climate models were forced with the CORE normal year (CNY) dataset and represent an average 1990 - 2015 climatology (Brickman et al. 2016; Wang et al. 2019). Future models for 2055 and 2075, RCP 4.5 and RCP 8.5 pathways were forced by adding IPCC circulation model anomalies to the CNY data (Brickman et al. 2016). Monthly covariates selected from the Brickman dataset for use were mixed layer depth (MLD), horizontal and vertical current velocity (U and V), bathymetry (bottom depth), sea surface and sea bottom temperature (SST and Sbtm), and sea surface and sea bottom salinity (SSS and Sbtm).

2.3. Zooplankton abundance data

We obtained *Calanus finmarchicus* and *Calanus hyperboreus* abundance data ($ind \cdot m^{-2}$) from the National Oceanic and Atmospheric Administration (NOAA) Fisheries Ecosystem Monitoring Program (EcoMon/MARMAP, hereafter referred to as EcoMon) survey (https://www.st.nmfs.noaa.gov/copepod/time-series/us-50101/) and the Fisheries and Oceans Canada (DFO) Atlantic Zone Monitoring Program (AZMP) (Maillet et al. 2019; Casault et al. 2020; Blais et al. 2021) (Figure 1). We chose to subset the available abundance data to the years 1990 through 2015 to correspond with the years represented by Brickman present-day covariates. EcoMon surveys sampled zooplankton using a 333 μm mesh net to a maximum depth of 200m; data has been collected since 1977 in the Gulf of Maine and south to the Mid-Atlantic Bight using random sampling techniques (Kane 2007; Richardson et al. 2010). AZMP samples were obtained using a 202 μm mesh net through the entire water column; data

was collected at stations since 1999 in the Labrador, Newfoundland, and Scotian shelves and slope waters as well as the Gulf of Saint Lawrence and Gulf of Maine (Therriault et al. 1998). We considered only late-stage abundance data (i.e., C4 through adult) for both *C. finmarchicus* and *C. hyperboreus* where possible because these lipid-rich stages are the primary target of *E. glacialis* foraging and most effectively caught in *E. glacialis* baleen plates (Mayo et al. 2001; Sorochan et al. 2019; Plourde et al. 2019; Lehoux et al. 2020). For the *C. hyperboreus* model, staged abundance data was not available in the EcoMon dataset and so we used unstaged totals. Although *C. hyperboreus* has been observed to reproduce in the Gulf of Maine (Conover 1967), there is evidence that reproduction primarily occurs further north in the GSL (Herman et al. 1991, Head et al. 1999) and *C. hyperboreus* abundance is relatively low in the GoM. This suggests that the inclusion of C1-C3 individuals in the GoM may have little effect on abundance counts. For the *C. hyperboreus* dataset, we also removed 137 records from the AZMP dataset with high Tbtm (> 5°C) along select transects and stations on the SS. These points represent outliers due to transport or possible errors in the dataset (Brennan et al. 2019).

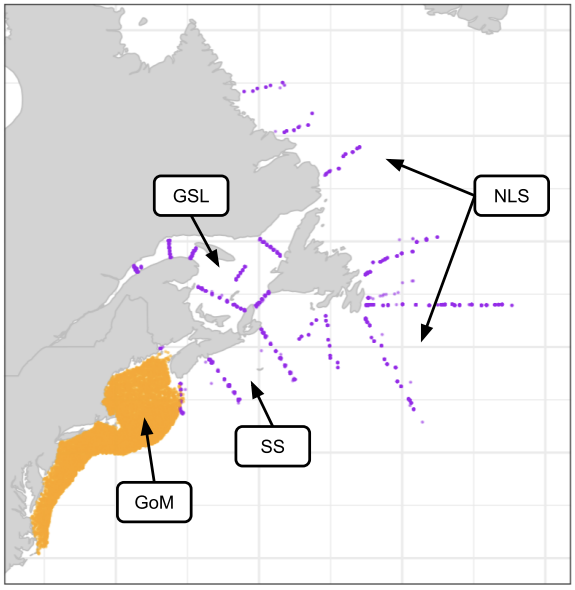

Figure 1. Map of Calanus *spp. sampling stations and regions colored by survey program. Orange represents points from the National Oceanic and Atmospheric Administration's (NOAA's) Fisheries Ecosystem Monitoring Program (EcoMon) survey and purple represents points from the Fisheries and Oceans Canada (DFO) Atlantic Zone Monitoring Program (AZMP). Regions indicated by labels are the Gulf of Maine (GoM), Scotian Shelf (SS), Gulf of St. Lawrence (GSL), and Newfoundland and Labrador Shelves (NLS).*

Since the EcoMon data only samples at most 200m of the water column, abundance data may be underestimated in regions with deeper bathymetry (e.g., off-shelf regions; termed "partial-water-column samples"). To correct underestimations in partial-water-column samples, we constructed a Generalized Additive Model (GAM) that predicted the proportion of total late-stage *C. finmarchicus* abundance sampled at a station (similar to Sorochan et al. 2019). *C. hyperboreus* did not have a vertical distribution correction applied due to a lack of sampling depth data and previously mentioned low abundance counts. The GAM was built with stratified

AZMP abundance data and used depth, month, and percent of the water column sampled as covariates. The GAM was applied to EcoMon points where station bathymetry was greater than 200m and the sampling depth was more than 15m above bathymetry (9.48% of the dataset). GAM performance degraded past 500m and so EcoMon points with bathymetry deeper than 500m were removed from the *C. Finmarchicus* dataset (18 points removed). By dividing summed late-stage abundance counts by GAM-estimated proportions, we derived corrected late-stage *C. Finmarchicus* abundance estimates for partial-water-column samples (Figure 3).

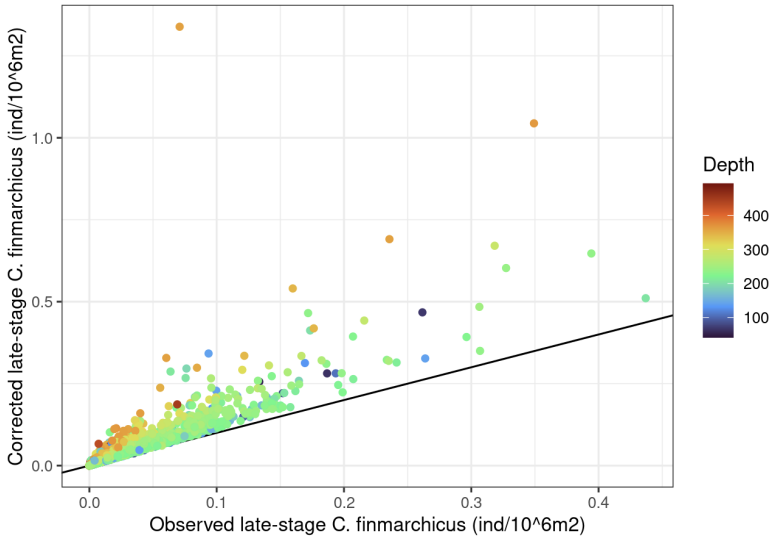

Figure 3. Effect of vertical distribution correction on C. finmarchicus *abundance. Observed late-stage* C. finmarchicus *abundance versus corrected late-stage* C. finmarchicus *as determined by the vertical correction GAM. The color of each point represents station bathymetry. Only corrected points (9.48% of the total EcoMon dataset) are displayed.*

2.4. Foraging habitat conversion

We converted *Calanus* spp. density data to suitable foraging habitat by implementing a critical feeding threshold: a depth-varying aggregated *Calanus* spp. density at which foraging becomes energetically viable for *E. Glacialis*. Points with density above the threshold are considered suitable feeding habitats for *E. glacialis* (hereby referred to as a “patch”). In order to apply a single energetic threshold to both *C. finmarchicus* and *C. hyperboreus* while acknowledging differences in size, we converted abundance data to estimated biomass using stage, species, and region-specific individual dry weight estimates from Sorochan et al. (2019) (Table 1). The vertical correction output does not provide stage-specific abundances, so C5 dry weight estimates were applied to the merged abundance counts. C5 dry weight estimates were chosen as the representative stage because their size is mid-range relative to C4 and C6 individuals and, for *C. finmarchicus*, also the most lipid-rich stage for *E. glacialis* (Sorochan et al. 2019).

Table 1. IDW ($\mu g \cdot ind^{-1}$) estimates of stage C5 used to derive biomass from late-stage abundance counts. Separated by species and region. Sourced from Sorochan et al. (2019).

Taxon / Region	GoM, SS	GSL, NLS
C. finmarchicus	195	333
C. hyperboreus	1145	1390

We developed a piecewise linear function to represent critical biomass density as a function of bathymetry (Figure 3). Although some research has been conducted to observe and determine *E. glacialis* feeding thresholds (e.g., DeLorenzo Costa et al. 2006; Baumgartner and Mate 2003; Plourde et al. 2019), most estimates are region-specific and there is no clear agreement on bioenergetic requirements. Ross et al. (in press) identifies *C. finmarchicus* abundance thresholds of 10,000 and 40,000 $ind \cdot m^{-2}$ as ideal thresholds for accurately modeling *E. Glacialis* foraging habitat in the GoM using a random forest model. These thresholds were based on empirical and observational ecological evidence and so can reasonably apply to other modeling algorithms, especially a comparable algorithm such as boosted regression trees (Li and Wang 2013; Ross et al. in press). We chose to adapt the 40,000 $ind \cdot m^{-2}$ threshold as a base value because it provided more ecologically justifiable, realistic predictions (Ross et al. in press). We multiplied the 40,000 $ind \cdot m^{-2}$ value by the individual dry weight estimate of 195 $\mu g \cdot ind^{-1}$ for *C. finmarchicus* in the GoM (Table 1) to derive a base biomass threshold of $7.8 \cdot 10^6$ µg for bathymetry up to 300m. Beyond depths of 300m, density requirements should increase with depth due to decreased vertical density and increased *E. glacialis* bioenergetic requirements (Plourde et al. 2019; Gavrilchuk et al. 2020). We therefore implemented a linear increase of an additional 19500µm per each meter of depth over 300m. This slope value was chosen as it maximized the ecological viability of predictions. To apply the critical thresholds and generate the input dataset for modeling, the derived *Calanus* spp. biomass data was matched to the spatially nearest Brickman present-day environmental covariates from the same month as datapoint collection. For each species-specific datapoint, the critical biomass threshold was calculated from bathymetry and compared to the estimated biomass to determine patch presence and absences.

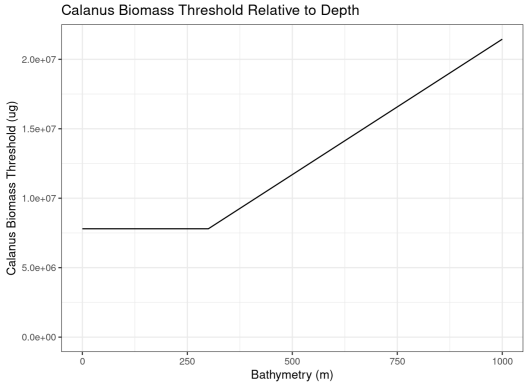

Figure 3. Calanus *spp. critical biomass feeding threshold versus bathymetry.*

The final *C. finmarchicus* and *C. hyperboreus* abundance datasets contained 19,222 and 21,344 points, respectively (Figure 4). Positive patch values made up 8.21% and 7.64% of the total points.

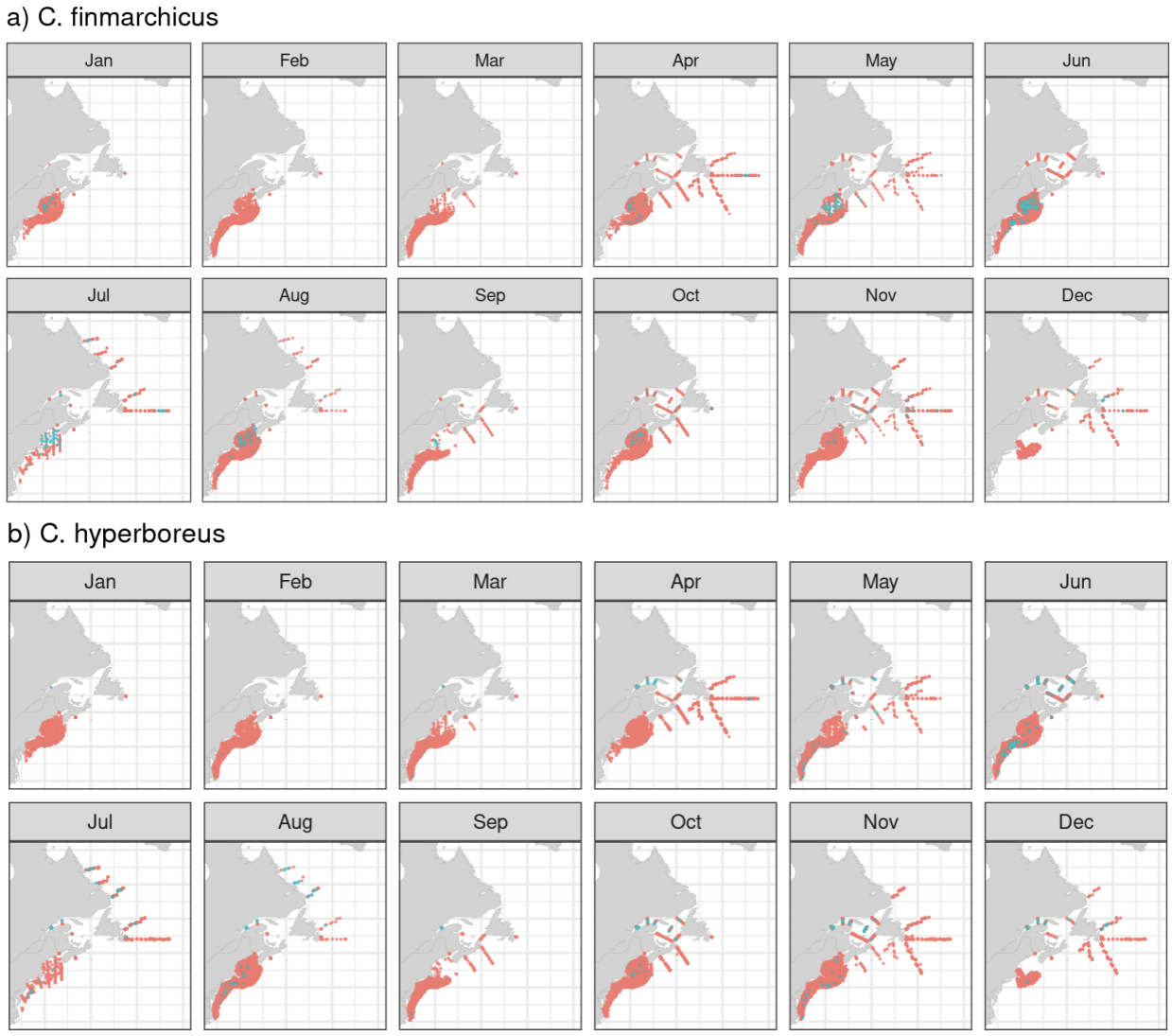

Figure 4. Maps of patch presences and absences by month and species. (a) Map of patch presences and absences for C. finmarchicus *by month. (b) Map of patch presences and absences for* C. hyperboreus *by month. Blue points indicate patch presences (areas where estimated dry weight is above the critical feeding threshold) and red points indicate absences.*

2.5. Species Distribution Modeling

Boosted regression tree classification models were trained on the patch presence/absence datasets and merged environmental covariates to create two separate models for *C. finmarchicus* and *C. hyperboreus*. Boosted regression trees generally have high predictive performance and allow for highly detailed responses, albeit with the potential for

overfitting (Elith et al. 2008, Ross et al. 2021). We created separate models for each species to allow for species-specific climatic responses. The boosted regression trees were built using the *tidymodels* and *xgboost* packages within R (Chen and Guestrin 2016). 75% of the dataset was used for training and 25% for testing, with the split stratified by patch. The predicted outcome variable was the probability of a feeding patch ranging between 0 and 1. All selected Brickman present-day covariates were used in the models, with the exception of SSS for the *C. hyperboreus* model. SSS was removed as a covariate from the *C. hyperboreus* model due to SSS's correlation with transport, a covariate that is not included in this study but affects *C. hyperboreus* distributions (Brennan et al. 2019). U and V were transformed into a single current velocity covariate (Vel) by the equation $Vel = sqrt(U^2 + V^2)$. Bathymetry was converted to a logarithmic scale (base 10). Additionally, all environmental covariates were normalized to have a mean of 0 and a standard deviation of 1. Boosted regression trees are capable of handling unnormalized data (Elith et al. 2008), but normalization allowed fair analysis of variable contribution using the *vip* package in R to evaluate absolute importance across all contributing trees in the ensemble (Greenwell and Boehmke). Month was included as a factored covariate to examine seasonality in model responses while maintaining consistency between monthly projections.

Models were tuned with inbuilt *tidymodels* functions to optimize the area under the receiver operating characteristic curve (AUC). AUC is a common method for evaluating SDMs and compares the proportions of correctly identified presences to incorrectly identified absences (Ross et al. 2021). AUCs above .5 indicate better performance than a random model (Fielding and Bell 1997) and are useful for estimating actual species distribution (Jiménez-Valverde 2012). The *C. finmarchicus* model was tuned by setting the number of trees to 1,000, tree depth to 12, learning rate to $6.84 \cdot 10^{-3}$, minimum n to 9, mtry to 6, sample size to .754, and loss reduction to $6.13 \cdot 10^{-9}$. The *C. hyperboreus* model was tuned by setting the number of trees to 1,000, tree depth to 7, learning rate to $1.77 \cdot 10^{-2}$, minimum n to 15, mtry to 4, sample size to .367, and loss reduction to $1.77 \cdot 10^{-8}$. To determine the confidence interval for the AUC, we trained and tested the models K = 100 times on different random splits of the dataset and calculated the 95% quantile range. Extracted monthly AUCs were derived for each model by calculating AUC for points in the testing dataset grouped by month.

We then projected the trained boosted regression tree models to the four future climate datasets from Brickman. "Patch shift maps" for each climate scenario displaying new and lost feeding habitats were created by observing how patch probabilities shift between present and future climate scenarios relative to a "critical probability" of 33%. Combined maps of patch probability across both species were taken by calculating the probability of a patch of either or both species at a point. We focus our conclusions on projections for the most extreme climate scenario, RCP85 2075, to highlight responses to extreme climate change.

3. Results

3.1. Model Performance

The *C. finmarchicus* model had an AUC of .909, which falls between the 95% quantile confidence interval (.889 - .912, K = 100 repeats). The *C. hyperboreus* model had an AUC of .919, which also falls between the 95% quantile confidence interval (.906 - .930, K = 100 repeats). Extracted monthly AUCs had consistently useful performance through the months of April through December, with averaged AUCs and confidence intervals above .7 (Pearce and Ferrier 2000) (Figure 5). During March in the *C. finmarchicus* model and from January through March in the *C. hyperboreus* model confidence intervals ranged below the .7 threshold for useful performance (Figure 5; Pearce and Ferrier 2000). For most of the results below, we show only January, March, July, and October to represent seasonality.

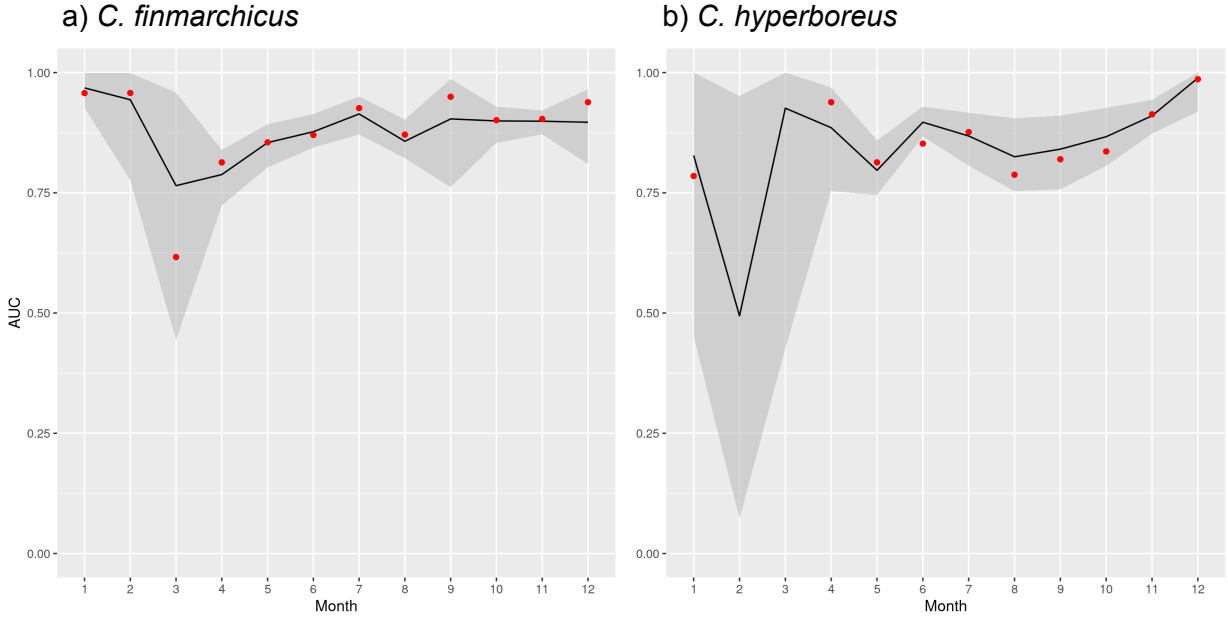

Figure 5. Area under the curve (AUC) mean and confidence interval by month for a) C. finmarchicus *and b)* C. hyperboreus*. Monthly values were derived by computing AUC from predictions in the testing dataset matching the desired month. Mean and 95% confidence interval by quantile are calculated for K = 100 repeats. Red dots indicate extracted monthly AUCs of the final model.*

The *C. finmarchicus* and *C. hyperboreus* modeled patch probabilities for present-day were moderately and loosely correlated to the underlying dry weight data (Figure 6; Spearman correlation coefficients of .6044 and .4733, respectively). GAMs fit to the patch probability versus dry weight data showed a general increasing trend in *C. finmarchicus* model response to higher dry weight (Figure 6a). For *C. hyperboreus*, the GAMs demonstrated increasing probability with dry weight until a biomass of roughly $10^{7.5}$ µg, after which patch probability declined (Figure 6b).

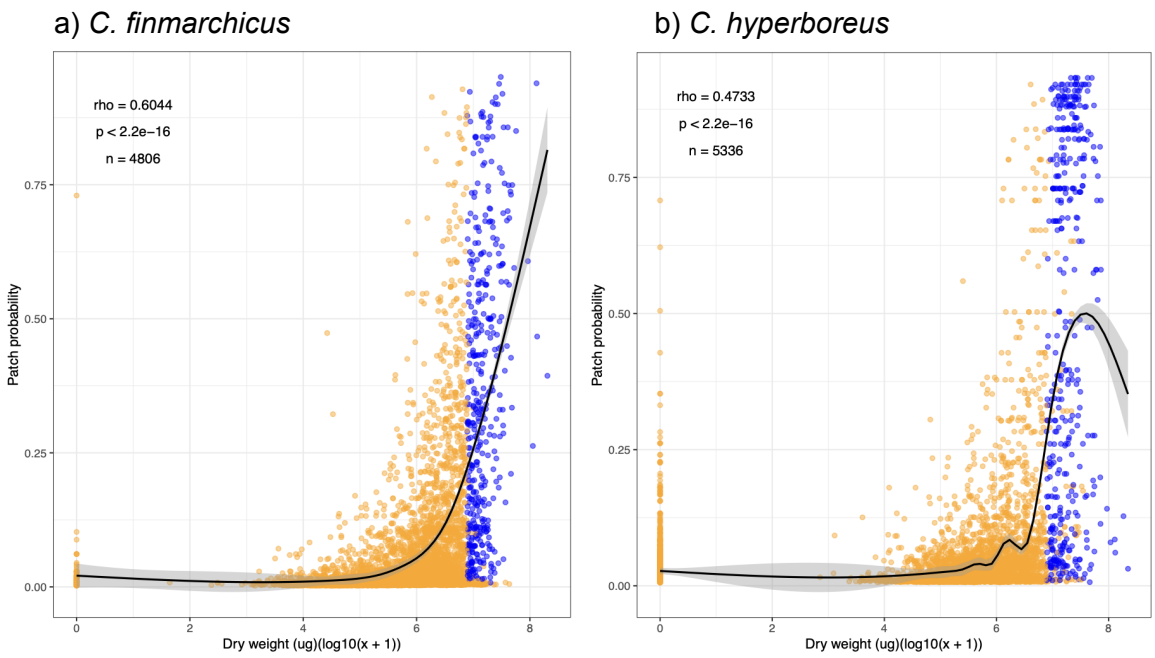

Figure 6. Scatter plots of measured dry weight ($log_{10}(x+1)$) versus modeled patch probability for a) C. finmarchicus *and b)* C. hyperboreus. *Blue points represent dry weight records measured as a patch, while orange points represent dry weight records measured as no patch. Spearman's correlation coefficient (rho), p-values, and sample size are superimposed on each plot. The black line and shaded regions represent the estimate and confidence interval for a GAM fitted to the data using a cubic spline.*

3.2. Variable Contribution and Response Curves

Covariate contributions varied between species (Figure 7). In the *C. finmarchicus* model, bathymetry and bottom salinity contributed most to the model, with current velocity contributing the least and all other variables contributing roughly equally (Figure 7a). In the *C. hyperboreus* model, bottom temperature and mixed layer depth had the highest contribution, with each subsequent variable having a smaller contribution down to current velocity, which had less than 5% importance (Figure 7b).

Response curves also varied between species models (Figure 8). *C. finmarchicus* displayed a strong relationship to bathymetry, with high patch values only expressed at bathymetric depths between 100 and 500 meters (Figure 8a). The model also expressed decreasing relationships between patch probability and all other variables except for bottom salinity, for which it displayed higher patch probabilities at values further away from the median (Figure 8a). The *C. hyperboreus* response curves conversely displayed an increasing relationship between patch probability and all variables, with the exceptions of mixed layer depth and current velocity for which it displayed a decreasing relationship (Figure 8b). Individual folds showed generally similar responses in the *C. finmarchicus* model, but had greatly varying intercepts in the *C. hyperboreus* model with the exception of mixed layer depth (Figure 8).

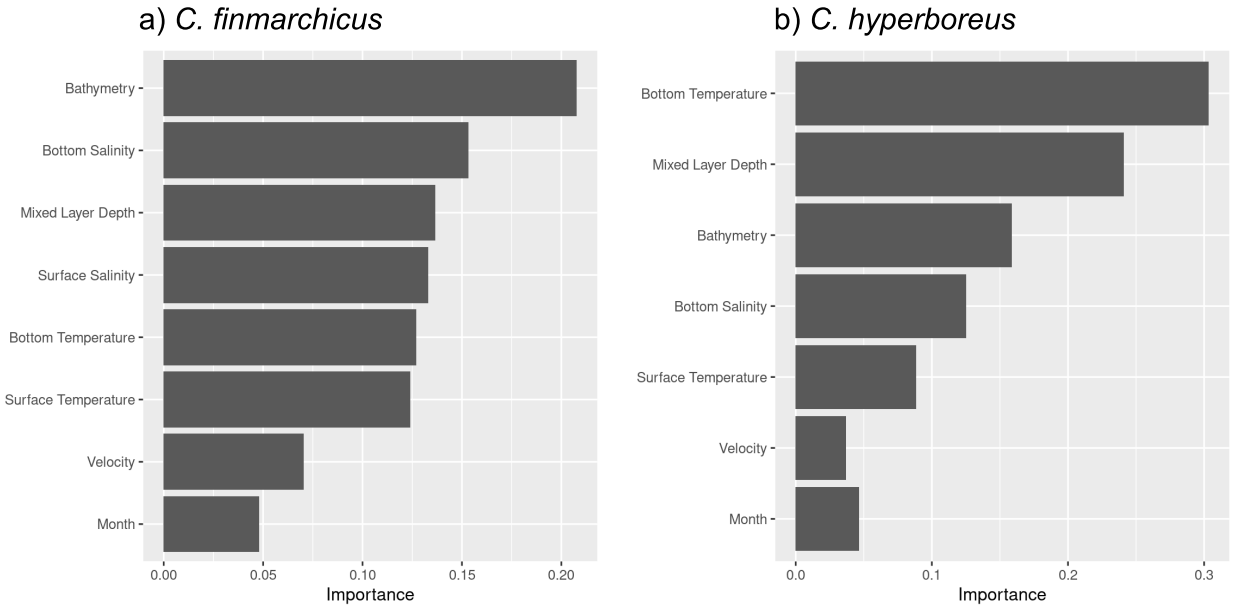

Figure 7. Variable importance for a) C. finmarchicus *and b)* C. hyperboreus as *determined by absolute magnitude of importance across BRT ensemble trees. Variable importance for Month is aggregated across 12 dummy variables and regarded as an artifact.*

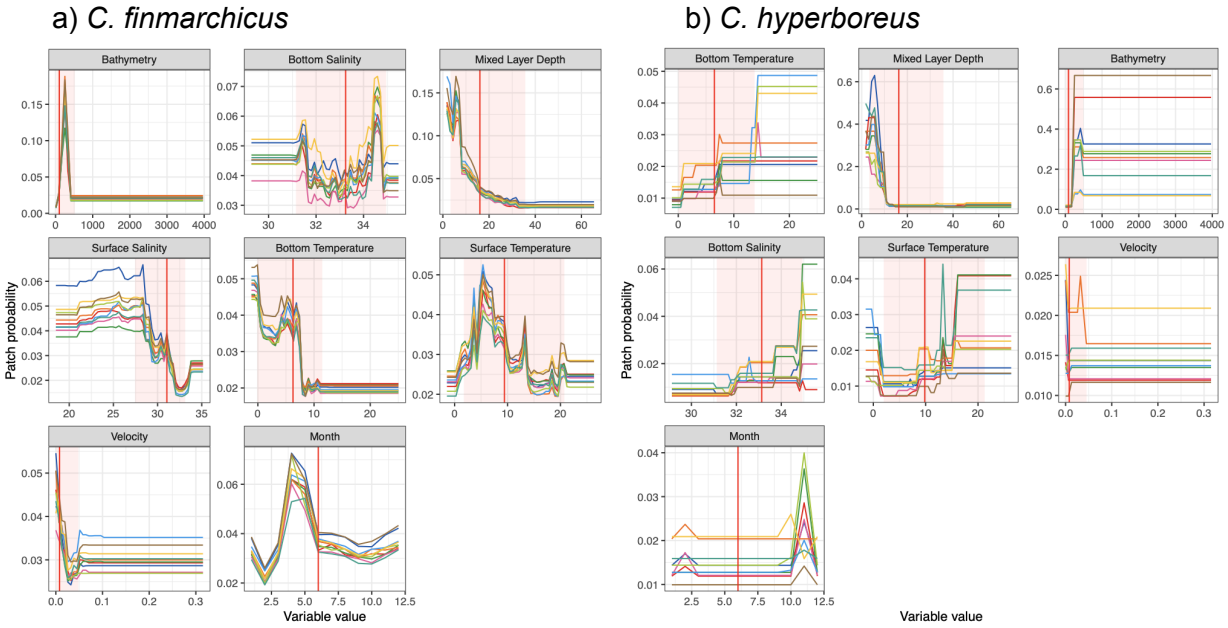

Figure 8. Response curves for a) C. finmarchicus *and b)* C. hyperboreus *model by covariate over 10 cross-validation folds. Red vertical lines and shaded areas indicate the median value and 95% quantile of the covariate within the training data range. Each line represents an individual fold's response to variation over the variable range while all other variables are held at median value (Elith et al. 2005).*

3.3. C. finmarchicus projections

The *C. finmarchicus* model present-day projections closely followed the *C. finmarchicus* patch data used to train it (Figure 9). High suitability in the GoM, Flemish Cap, and the central SS were predicted during the months of May to July (Figure 9c). Moderate areas of patch suitability were identified along the edges of the continuous northeast shelf, the edges of the Laurentian channel, some portions of the southwestern GSL, and the Roseway basin (Figure 9c). Model predictions varied monthly, with greatly decreased patch suitability indicated from December through April.

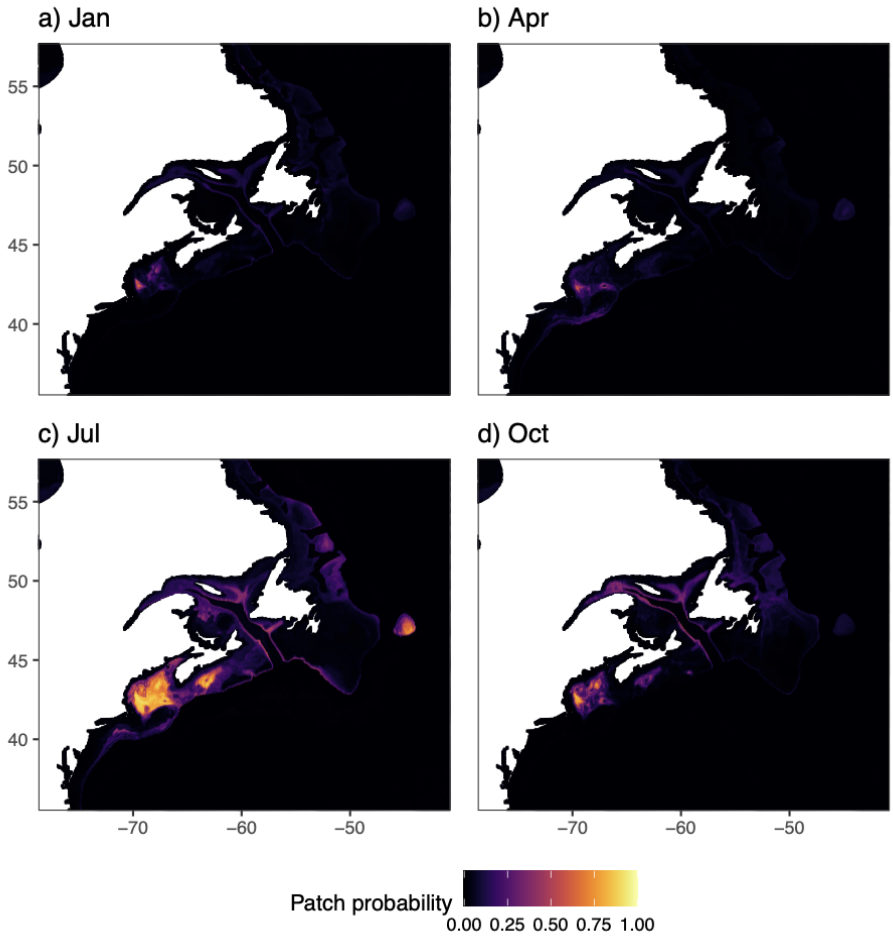

Figure 9. Predicted C. finmarchicus *patch probability for present-day Brickman et al. (2021) modeled environmental covariates during the representative months of January, April, July, and October.*

We chose to focus our comparisons between future climate scenarios to the month of July and RCP85 2075, the most extreme climate scenario, as an illustrative example (Figure 10). There were moderate differences between predictions for each climate scenario, with the greatest differences observed between RCP45 2055 and RCP85 2075 projections (Figure 10a, 10d). The RCP scenario modeled appeared to have more of an influence on model output than

the year (Figure 10). In general, later years and higher RCP scenarios lowered patch probability on the GoM, Flemish Cap, and shelf edges and mildly increased patch probability in the GSL and eastern SS (Figure 10).

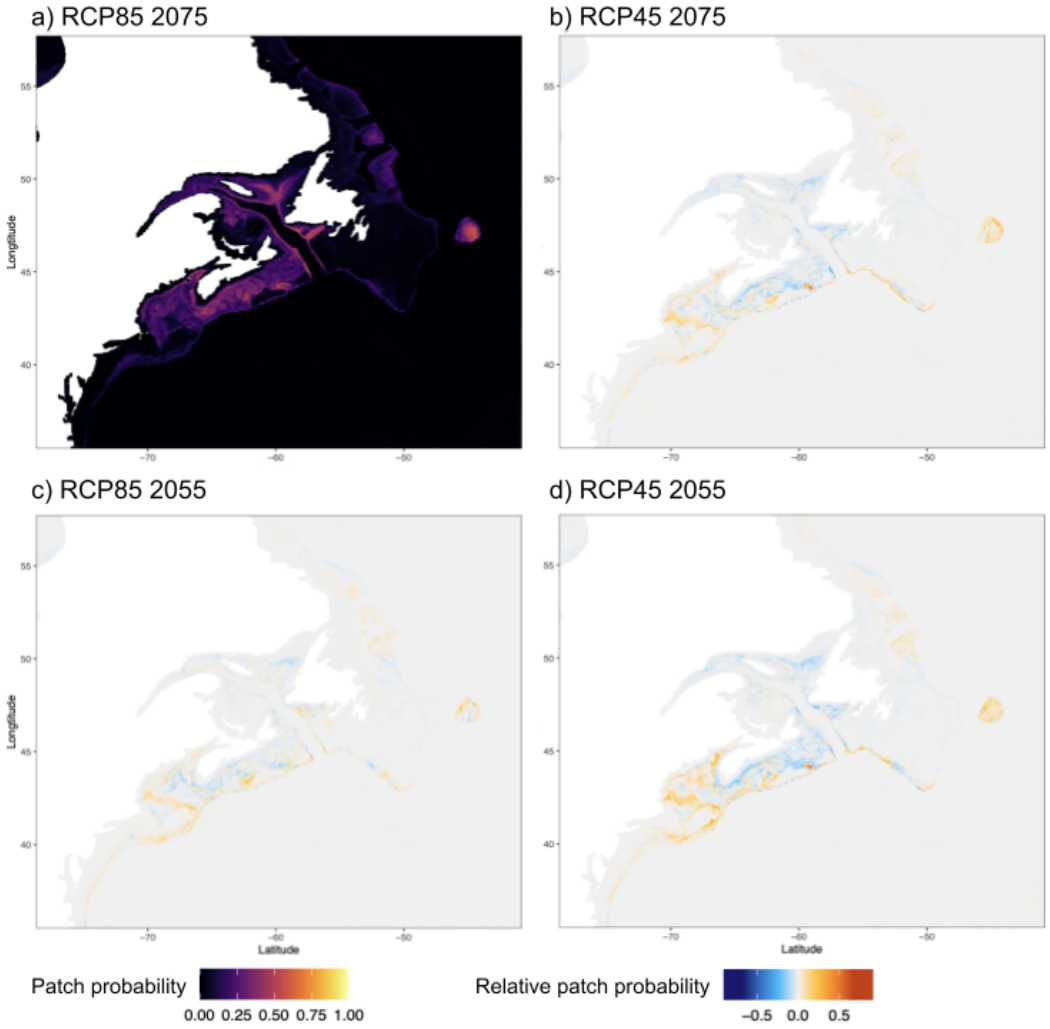

Figure 10. Predicted C. finmarchicus *patch probability across future climate scenarios during the representative month of July. a) Predicted patch probability for 2075 under IPCC representative concentration pathway 85 (RCP85) in July. b-d) Predicted patch probability expressed as the difference from RCP85 2075 projections for b) RCP45 2075, c) RCP85 2055, and d) RCP45 2055 in July. Orange areas indicate higher patch probability and blue represents lower patch probability.*

Patch shift maps for RCP85 2075 highlight areas of new, lost, and retained *C. finmarchicus* feeding habitat (Figure 11). Across all months, most of the feeding habitat in the GoM was lost, with the exception of new and retained feeding habitats on the eastern edge and Bay of Fundy during the summer (Figure 11). New feeding habitat was projected within the Roseway basin, eastern SS, and along the edges of the Laurentian Channel (Figure 11).

Summer feeding habitat in the Flemish cap was also retained, although with some habitat loss at the edges (Figure 11c).

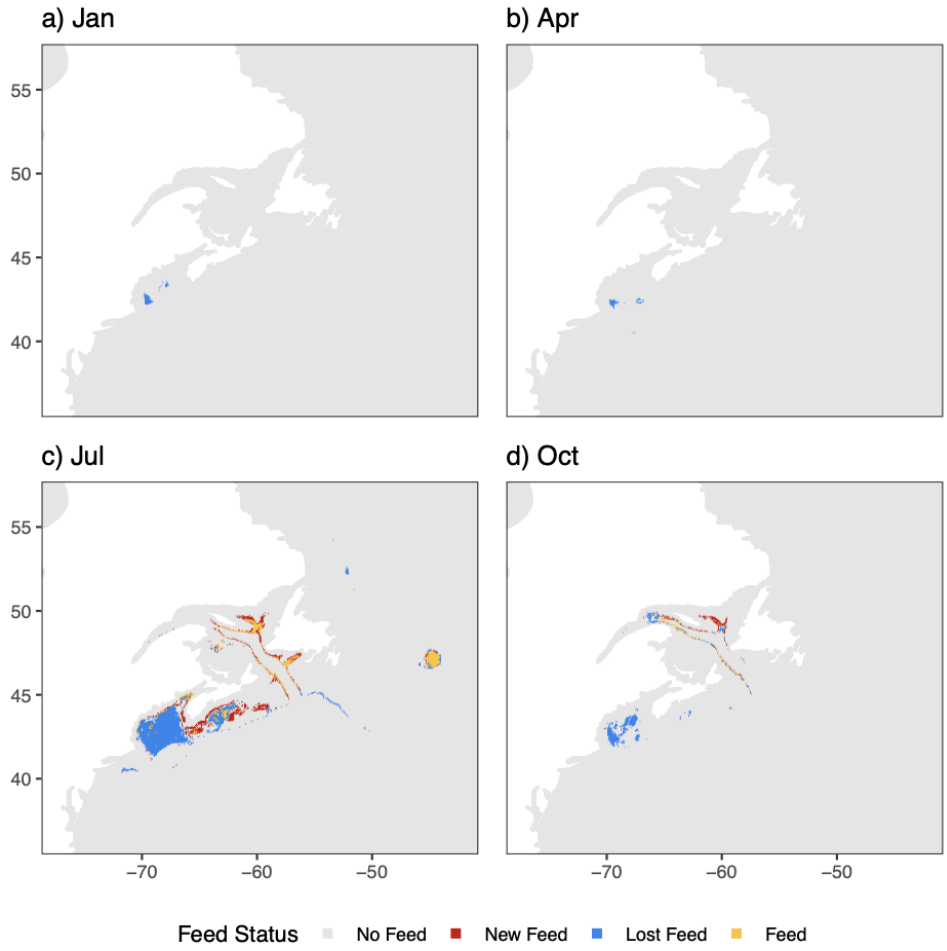

Figure 11. Patch shift maps for C. finmarchicus *in 2075 under representative concentration pathway (RCP) 85 during the representative months of January, April, July, and October. The color at a point represents how patch probability shifted between present day and RCP85 2075 predictions relative to a critical probability of 33.3%. Yellow 'Feed' indicates points that remained above the critical threshold, gray 'No Feed' indicates points that remained below the threshold, blue 'Lost Feed' indicates points that dropped from above to below the threshold, and red 'New Feed' indicates points that moved from below to above the threshold.*

3.4. C. hyperboreus projections

The *C. hyperboreus* model present-day projections also followed recorded patch presences and absences (Figure 12). Very high suitability was recorded at the northwestern GSL year-round, with moderate suitability around the edges and northeastern end of the Laurentian channel that increased during the summer and fall (Figure 12). The southwestern GSL also had moderate suitability during June and July (Figure 12c). During the summer,

mid-high suitability was projected on the NLS, particularly in shallower areas (Figure 12d). This area of suitability shrank during the fall (Figure 12d). Little to no *C. hyperboreus* probability was recorded in the SS or GoM despite some positive patch values in the dataset (Figure 12).

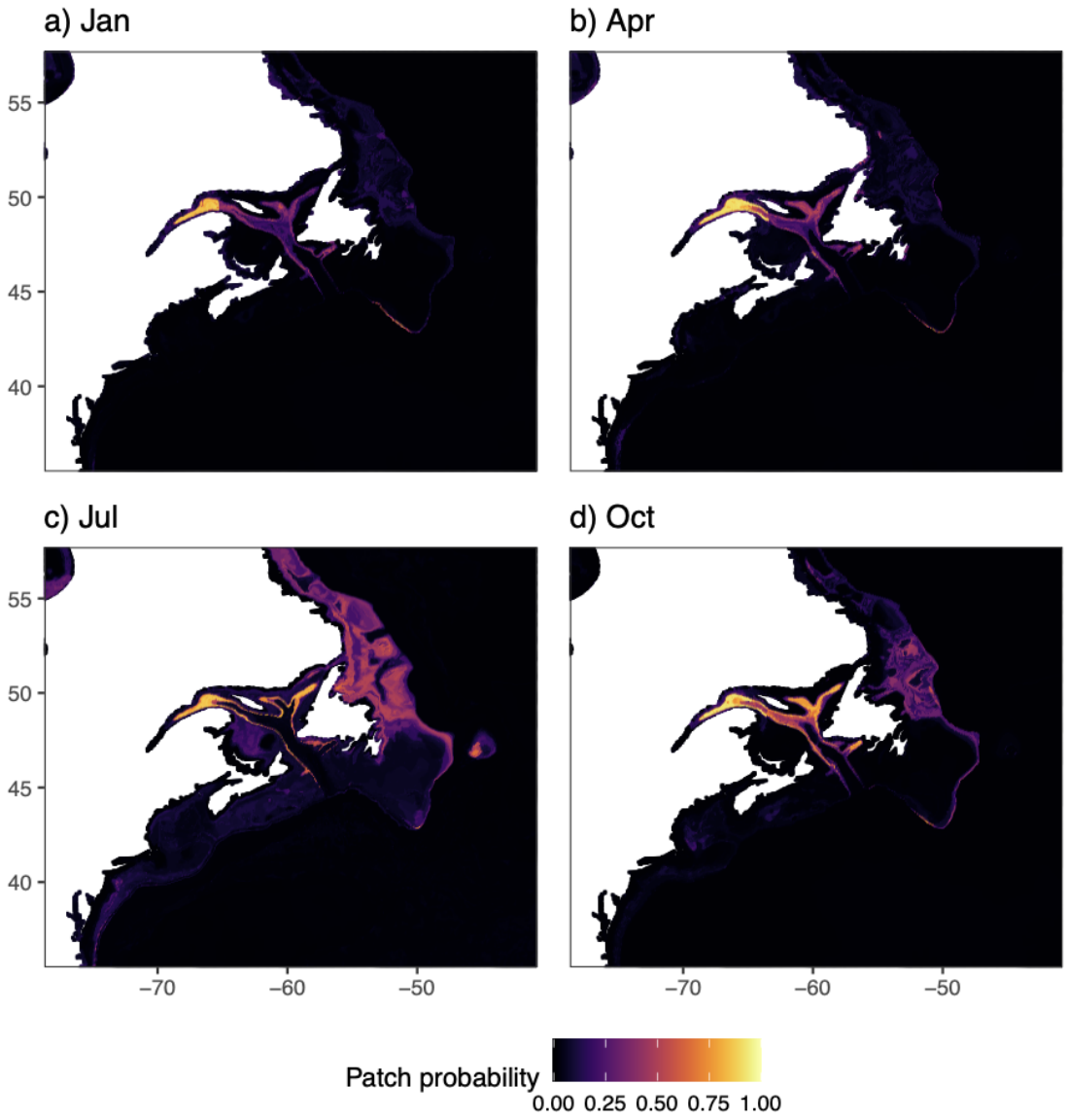

Figure 12. Predicted C. hyperboreus *patch probability for present-day Brickman et al. (2021) modeled environmental covariates during the representative months of January, April, July, and October.*

Comparisons between future climate scenarios had similar variability to the *C. finmarchicus* model (Figure 13). Changes between climate scenarios were mild overall, with the greatest differences observed between RCP45 2055 and RCP85 2075 projections (Figure 13a, 13d). Like the *C. finmarchicus* model, the RCP scenario also had more influence on model output than the year (Figure 13). General trends predicted that later years and higher RCP scenarios would lower patch probability in the GoM and central NLS and increase patch

probability on the edges of the contiguous northeast shelf (Figure 13). Both of the RCP45 models also showed greatly increased patch probability at the northwest and northeast tips of the Laurentian Channel relative to the RCP85 2075 scenario (Figure 13b, 13d).

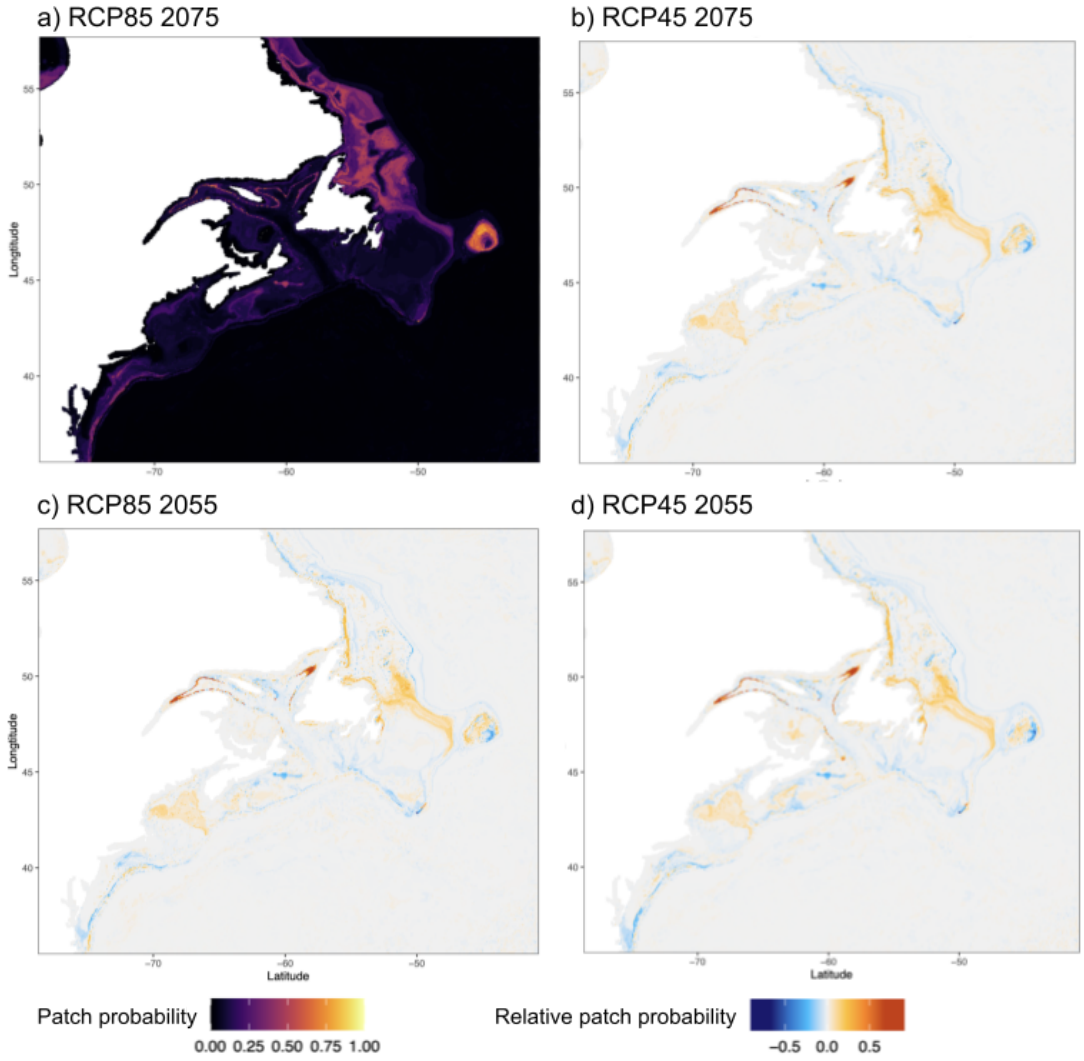

Figure 13. Predicted C. hyperboreus *patch probability across future climate scenarios during the representative month of July. a) Predicted patch probability for 2075 under IPCC representative concentration pathway 85 (RCP85) in July. b-d) Predicted patch probability expressed as the difference from RCP85 2075 projections for b) RCP45 2075, c) RCP85 2055, and d) RCP45 2055 in July. Orange areas indicate higher patch probability and blue represents lower patch probability than RCP85 2075 projections.*

Patch shift maps for RCP85 2075 highlight areas of new, lost, and retained *C. hyperboreus* feeding habitat (Figure 14). Projected changes exhibited significant seasonality. The northeast tip of the Laurentian channel was projected as a retained feeding habitat through all seasons except Summer, during which it was lost (Figure 14c). The rest of the Laurentian channel exhibited greatly reduced habitat (Figure 14). In the NLS regions habitat suitability was

mostly retained or added, especially during the summer and fall; however, there were also some regions of loss during the summer along the coastline and the central shelf (Figure 14c).

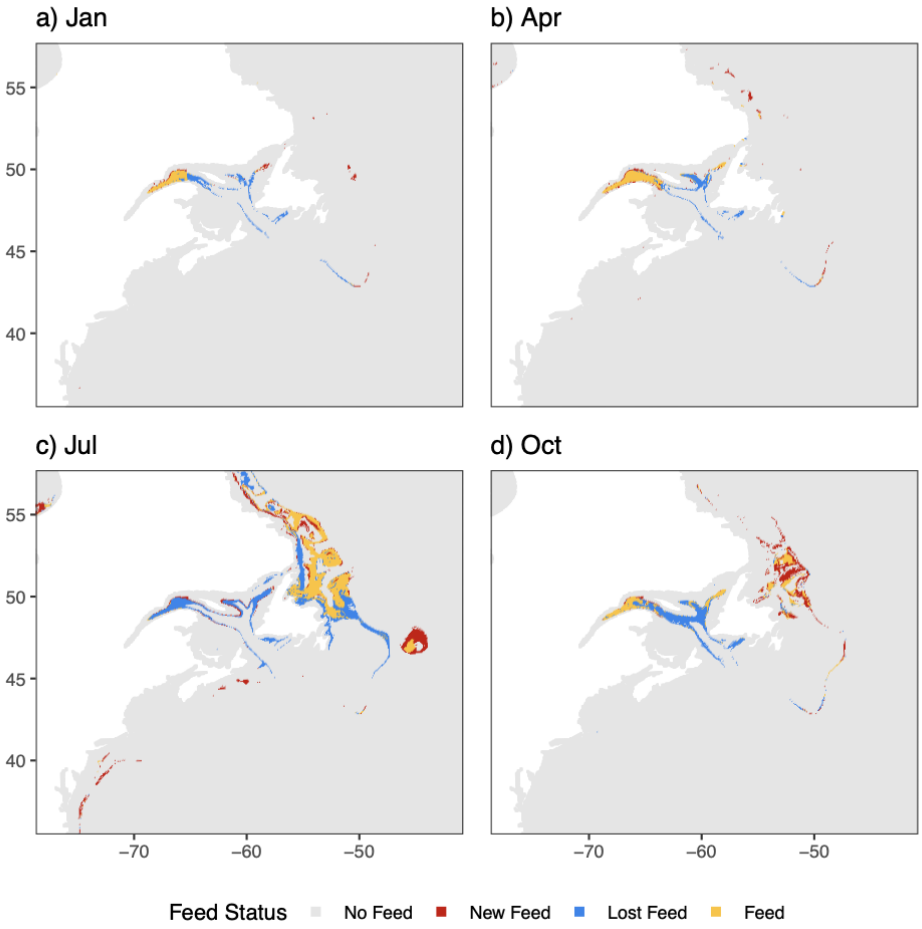

Figure 14. Patch shift maps for C. hyperboreus *in 2075 under representative concentration pathway (RCP) 85 during the representative months of January, April, July, and October. The color at a point represents how patch probability shifted between present day and RCP85 2075 predictions relative to a critical probability of 33.3%. Yellow 'Feed' indicates points that remained above the critical threshold, gray 'No Feed' indicates points that remained below the threshold, blue 'Lost Feed' indicates points that dropped from above to below the threshold, and red 'New Feed' indicates points that moved from below to above the threshold.*

3.5. Combined projections

Combined predictions for present-day *E. glacialis* feeding habitat considered suitable areas where either or both species had high patch suitability (Figure 15). In areas where only one species had high patch suitability, such as the NLS or the GoM, projections closely mapped to the respective source species (Figure 15). In areas with overlapped suitability, such as the GSL, patch suitability increased. In particular, the southwestern GSL and eastern SS both

displayed higher patch probability in the combined plots during the summer than either species had projected alone (Figure 15c).

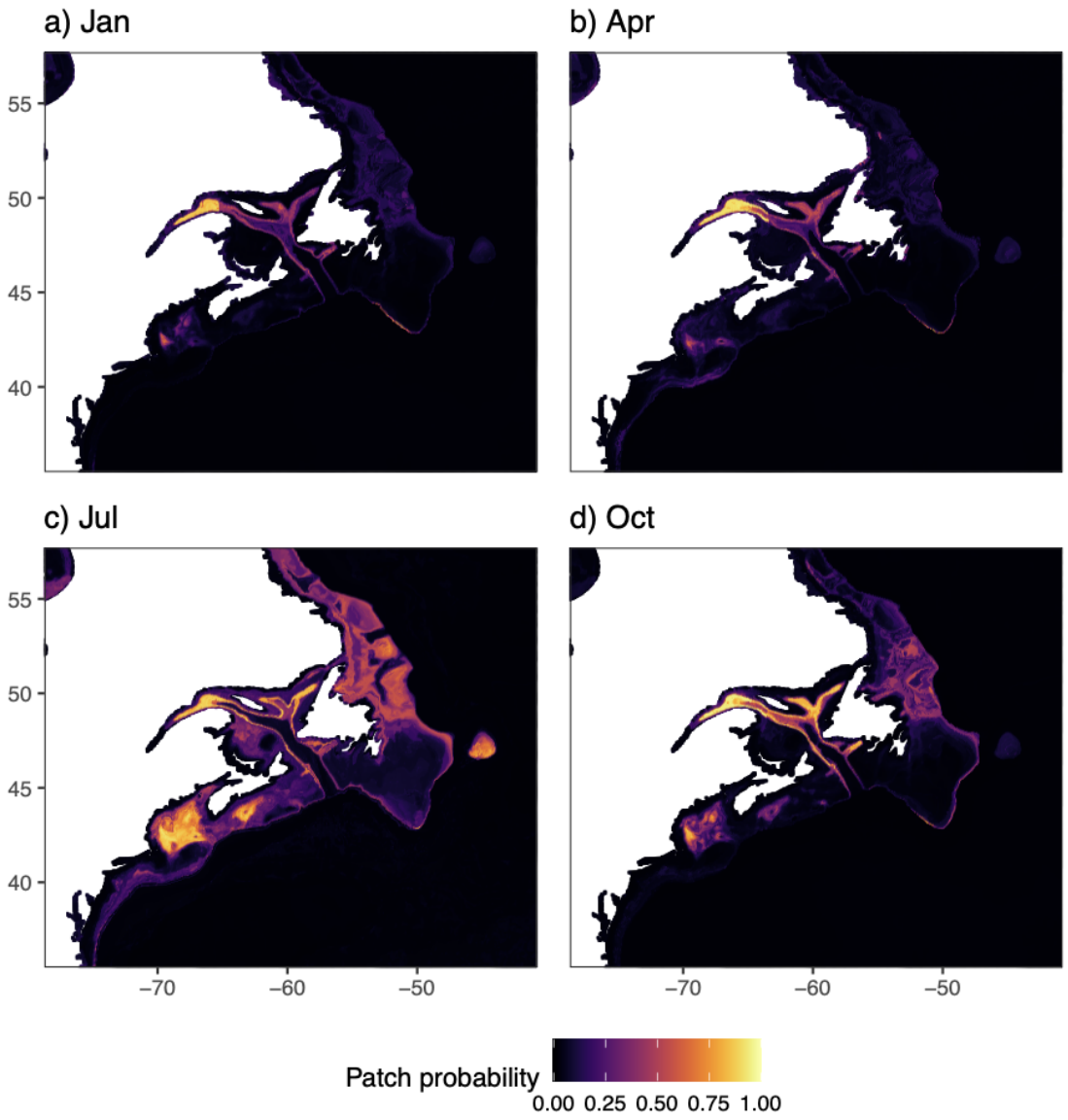

Figure 15. Predicted Calanus spp. *patch probability for present-day Brickman et al. (2021) modeled environmental covariates during the representative months of a) January, b) April, c) July, and d) October. Patch probability is expressed on a color bar scaling from 0 to 1 and represents the combined probability of any species patch.*

Combined patch shift maps likewise displayed some elements from both the *C. finmarchicus* and *C. hyperboreus* plots (Figure 16). Lost feeding habitat was projected within most of the GoM, although some habitat in the central GoM was retained during the summer (Figure 16c). Retained and increased habitat suitability was projected across the SS and NLS, similar to the *C. finmarchicus* and *C. hyperboreus* models (Figure 16). Within the GSL, areas of

retained and lost habitat suitability were similar to the *C. hyperboreus* projections during the fall, winter, and spring, although with increased areas of retained habitat on the upper ends of the Laurentian Channel (Figure 16a, 16b, 16d). However, summer habitat around the edges of the Laurentian channel was retained, similar to the *C. finmarchicus* projections (Figure 16c).

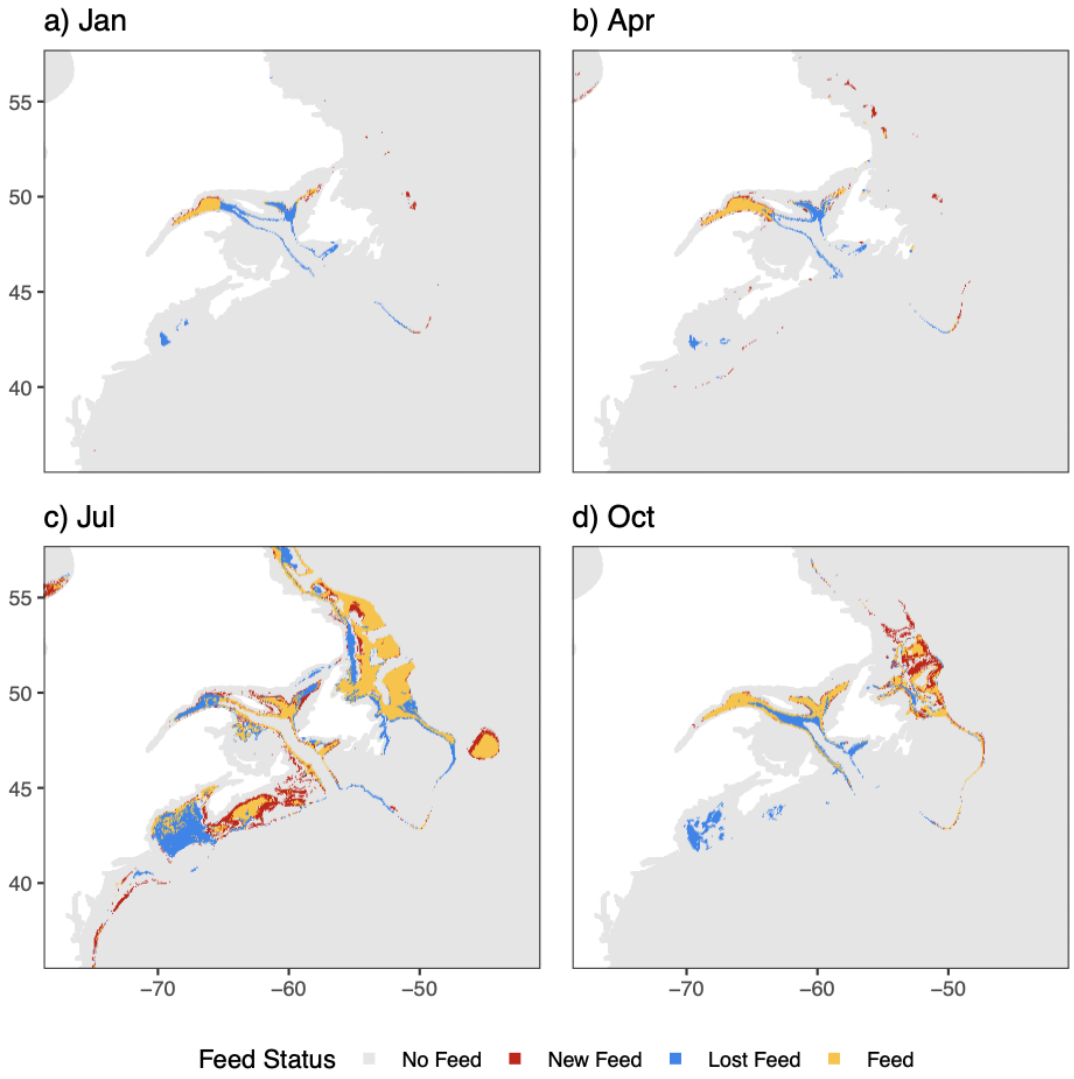

Figure 16. Patch shift maps for combined C. hyperboreus *and* C. finmarchicus *in 2075 under representative concentration pathway (RCP) 85 during the representative months of January, April, July, and October. Combined patch probability was evaluated as the probability of a patch of either or both species at a point. The color at a point represents how combined patch probability shifted between present day and RCP85 2075 predictions relative to a critical probability of 33.3%. Yellow 'Feed' indicates points that remained above the critical threshold, gray 'No Feed' indicates points that remained below the threshold, blue 'Lost Feed' indicates points that dropped from above to below the threshold, and red 'New Feed' indicates points that moved from below to above the threshold.*

4. Discussion

In this study, we examined present and future *E. glacialis* feeding distributions by modeling suitable foraging habitats, derived by comparison between measured *Calanus* spp. biomass and a critical feeding threshold, to modeled environmental covariates. We then projected these results to 2055 and 2075 for RCP45 and RCP85 scenarios to examine how *E. glacialis* feeding habitats may shift due to climate change.

Both the *C. finmarchicus* and *C. hyperboreus* models showed generally high performance according to their AUC (Pearce and Ferrier 2000). Extracted monthly AUCs showed moderate to high performance during the summer and fall, which are seasons during which *E. glacialis* historically feeds (Ross et al. 2021). *C. finmarchicus* extracted AUCs are high during the winter months, but this may be due to a low number of sightings falsely inflating AUC scores. *C. hyperboreus* extracted monthly AUCs were low during winter months, corresponding to a lack of AZMP records. The fitted GAM for the *C. hyperboreus* dataset displayed a decreasing relationship between patch probability and dry weight at extremely high dry weight levels. The highest dry weight values are primarily observed in the Laurentian channel, which has deeper bathymetry than most other measured areas (Plourde et al. 2019); therefore the decreasing relationship at high abundance is likely due to the model's response to high bathymetry – i.e. in very deep waters *Calanus* spp. patches are no longer accessible to whales.

Variable contribution varied between species, demonstrating that the choice to model species separately allowed for variation in climatic responses. The most important variable in the *C. hyperboreus* model was bottom temperature, which was also a moderate contributor to the *C. finmarchicus* model. Although surface temperature is an extremely common covariate in *Calanus* spp. modeling (e.g. Pershing et al. 2009, Villarino et al. 2011, Grieve et al. 2017), the relative significance of bottom temperature in our model relative to surface temperature indicates that including bottom temperature or other subsurface metrics may reveal differing relationships and important subsurface processes. The importance of mixed layer depth in both models also suggests that its inclusion may improve model predictions, especially considering mixed layer depth's crucial role in aggregating copepod prey (Diaz et al. 2021). *C. finmarchicus* model responses to temperature also align with prior studies. The highest patch probabilities were observed at surface temperatures between 3° and 8°C, which is similar to the predicted favorable range of 4.5° - 8.5°C from Reygondeau and Beaugrand (2011). Patch probabilities also peaked at bottom temperatures near or below 0° C, which agrees with Grieve et al.'s (2017) modeled peaks at temperatures < 2°C. *C. hyperboreus* variable response curves showed some significant differences from the *C. finmarchicus* response curves, most notably with inverted relationships between bottom temperature, bottom salinity, and surface temperature. In particular, the observed increasing relationship between surface temperature and patch probability contrasts prior work that correlated increased surface temperature with lowered *C. hyperboreus* abundance (Sorochan et. al 2019). However, at low surface temperatures, the negative correlation was still observed, suggesting that at higher surface temperatures deeper water dynamics may have more influence on habitat.

Present day patch projections for *C. finmarchicus* foraging grounds were correlated with historical *E. glacialis* sightings during summer feeding months. For example, high *C. finmarchicus* patch probabilities were predicted in the Gulf of Maine throughout the summer and the Bay of Fundy during July and August, both of which are historically documented feeding grounds (Morison and Gaskin 1989, Baumgartner and Mate 2003). Additional areas in the central and western Scotland Shelf were also highlighted which have had limited historical survey effort but were identified as likely present day feeding ground by other models (e.g. Plourde al. 2019, Ross et al. in press). Present day projections for *C. hyperboreus*, while outside historical *E. glacialis* survey efforts, were correlated with shallower areas known to have high *C. hyperboreus* abundances such as the edges of the Laurentian channel and the Newfoundland and Labrador shelves (Head and Pepin 2010). The areas on the Laurentian Channel within the GSL were also indicated as suitable feeding habitats by Plourde et al. (2019). *C. hyperboreus* patch probabilities were also extremely low both on and below the Scotian Shelf. Although *C. hyperboreus* does inhabit areas on the SS, it is mainly considered as an emigrant from the GSL and so our model, which does not consider transport as a covariate, may reasonably ignore high abundance in this area (Herman et al. 1991, Sameoto and Herman 1992). The combined present-day forecasts indicated all of the high suitability regions mentioned as well as higher patch suitability on the eastern SS and southwestern GSL, both of which were indicated as likely suitable feeding grounds by Plourde et al. (2019). The additional high suitability areas indicated by combining *Calanus* spp. projections suggest that models considering multiple prey species could reveal crucial feeding habitats invisible to single-species models, especially in areas of overlapped prey distributions.

Projections to the most extreme climate scenario, RCP85 2075, shows significant areas of change to *E. glacialis* feeding habitat distributions. *C. finmarchicus* projections showed a large loss of feeding habitat year round throughout most of the GoM. The loss of habitat within the GoM has been projected by other studies considering *E. glacialis* feeding habitats or *C. finmarchicus* abundance data (e.g. Raygondeau and Beaugrand 2011; Grieve et al. 2017; Ross et. al 2021). New and retained feeding habitat was also indicated along portions of the Scotian Shelf, which was also reported by Ross et. al (2021). The smaller regions of new and retained suitability relative to lost feeding habitat suggest that suitable *C. finmarchicus* feeding areas for *E. glacialis* may reduce due to climate change, thus highlighting the importance of implementing conservation strategies in critical habitat. *C. hyperboreus* feeding patches also shifted in future climate scenarios, with reduced habitat in the Gulf of St Lawrence. These results contrast with prior studies which predict that *C. hyperboreus* may exhibit relatively less habitat shift than *C. finmarchicus* (Chust et al. 2014, Villarino et al. 2015). However, these studies do not consider *C. hyperboreus* abundance relative to potential *E. glacialis* feeding habitat and suggest that further examination of *C. hyperboreus* as a prey species for *E. glacialis* may reveal additional insight. The combined threshold maps show a similar loss of habitat in the GoM and an increase in the SS to the *C. finmarchicus* projections. However, during the summer and fall, the projections show wide areas retained habitat suitability in the GSL, suggesting that added *C. finmarchicus* abundance may compensate for any loss in *C. hyperboreus* habitat. High habitat suitability areas were also retained and expanded along the NLS and Flemish Cap, areas which have not been considered in prior *E. glacialis* modeling studies. Overall, the general northward shift of

suitable feeding areas corresponds to recent shifts in *E. glacialis* distributions (Davis et al. 2017; Meyer-Gutbrod et al. 2021), and the additional suitable areas in the NLS and Flemish Cap suggest the potential of further northward migration. Projected feeding areas did not see highly significant differences in projections between future years and representative concentration pathways, similar to the results reported by Grieve et al.'s (2017) study of *C. finmarchicus* abundance in future years.

Several factors may affect the robustness of our results. First, in regards to accurate modeling of *Calanus* spp. aggregations, the model does not include some potentially important abiotic factors for *Calanus* spp. distributions such as pH and transport. Ocean acidification may affect copepod life cycles (Cripps et al. 2014; Thor et al. 2016) and transport has been demonstrated as an important contributor to *C. hyperboreus* distributions around the GSL and SS (Brennan et al. 2019). Additionally, evolutionary adaptation is not considered. *C. finmarchicus* populations have shown poor adaptation to present temperature increases (Hinder et al. 2014); however, *C. hyperboreus* has been shown to adapt relatively well to climate change in the Arctic and so adaptation may have more of an effect on future distributions (Kvile et al. 2018). In regards to projecting *E. glacialis* habitat, the biomass conversion used assumes a static individual dry weight by species over two regions. However, *Calanus* spp. biomass has been demonstrated to have finer geographic variability and decreased IDW under higher temperatures in surface waters (Sorochan et al. 2019, Plourde et al. 2019). Although the relative shifts in biomass between regions and temperatures are relatively small, decreased biomass in warm conditions may mean that regions experiencing significant warming in future years have exaggerated habitat suitability in our model. The bioenergetic requirements for *E. glacialis* may also have similar variability by region and other environmental covariates (Plourde et al. 2019), although the exact effects have not been quantified with significant detail.

The goal of this modeling study was to identify potential *E. glacialis* feeding habitats at a fine resolution across its full international domain. These results indicate new areas where survey efforts could be directed to give an early warning of right whale distributional shifts – e.g. the SS, NLS, and Flemish cap, retained habitat in the GSL, and lost habitat in the GoM. Considering the disproportionate rate of warming in the Gulf of Maine (Pershing et al. 2015), these projected new habitats could become energetically viable at a nearer time frame than 2055 or 2075. Future studies considering additional prey species such as *Pseudocalanus* spp. and *Centropages* spp. may reveal additional habitats and improve predictions, especially during winter months when they are of increased importance (Mayo and Marx 1990; Ross et al. 2021). Additional inclusion of vertically resolved data and models (e.g. Plourde et al. 2019, Brennan et al. 2021) could reveal vertical trends in *E. glacialis* feeding distributions and prey aggregations. These results are a crucial step toward understanding the full extent of *E. glacialis* migration under climate change and suggest that additional modeling and consideration of northern areas will help mitigate future anthropogenic mortalities.

Literature Cited

Baumgartner, M. F., F. W. Wenzel, N. S. J. Lysiak, and M. R. Patrician. 2017. North Atlantic right whale foraging ecology and its role in human-caused mortality. Marine Ecology Progress Series **581**: 165–181.

Baumgartner, M., and B. Mate. 2003. Summertime foraging ecology of North Atlantic right whales. Mar. Ecol. Prog. Ser. **264**: 123–135. doi:10.3354/meps264123

Beardsley, R. C., A. W. Epstein, C. Chen, K. F. Wishner, M. C. Macaulay, and R. D. Kenney. 1996. Spatial variability in zooplankton abundance near feeding right whales in the Great South Channel. Deep Sea Research Part II: Topical Studies in Oceanography **43**: 1601–1625. doi:10.1016/S0967-0645(96)00050-1

Blais, M., P. S. Galbraith, S. Plourde, L. Devine, and C. Lehoux. Chemical and Biological Oceanographic Conditions in the Estuary and Gulf of St. Lawrence during 2019.

Brennan, C. E., F. Maps, W. C. Gentleman, and others. 2019. How transport shapes copepod distributions in relation to whale feeding habitat: Demonstration of a new modelling framework. Progress in Oceanography **171**: 1–21. doi:10.1016/j.pocean.2018.12.005

Brennan, C. E., F. Maps, W. C. Gentleman, D. Lavoie, J. Chassé, S. Plourde, and C. L. Johnson. 2021. Ocean circulation changes drive shifts in Calanus abundance in North Atlantic right whale foraging habitat: A model comparison of cool and warm year scenarios. Progress in Oceanography **197**: 102629. doi:10.1016/j.pocean.2021.102629

Brickman, D., M. A. Alexander, A. Pershing, J. D. Scott, and Z. Wang. 2021. Projections of physical conditions in the Gulf of Maine in 2050. Elementa: Science of the Anthropocene **9**: 00055. doi:10.1525/elementa.2020.20.00055

Byrd, B. L., T. V. N. Cole, L. Engleby, and others. 2016. US Atlantic and Gulf of Mexico marine mammal stock assessments - 2015.doi:10.7289/V57S7KTN

Casault, B., E. Devred, E. Head, A. Cogswell, and J. Spry. Optical, Chemical, and Biological Oceanographic Conditions on the Scotian Shelf and in the eastern Gulf of Maine during 2019.

Chen, T., and C. Guestrin. 2016. XGBoost: A Scalable Tree Boosting System. *Proceedings of the 22nd ACM SIGKDD International Conference on Knowledge Discovery and Data Mining*. Association for Computing Machinery. 785–794.

Chust, G., C. Castellani, P. Licandro, L. Ibaibarriaga, Y. Sagarminaga, and X. Irigoien. 2014. Are Calanus spp. shifting poleward in the North Atlantic? A habitat modelling approach. ICES Journal of Marine Science **71**: 241–253. doi:10.1093/icesjms/fst147

Conover, R. J. 1967. Reproductive Cycle, Early Development, and Fecundity in Laboratory Populations of the Copepod Calanus Hyperboreus 1). Crustaceana **13**: 61–72. doi:10.1163/156854067X00080

Conover, R. J. 1988. Comparative life histories in the genera Calanus and Neocalanus in high latitudes of the northern hemisphere. Hydrobiologia **167**: 127–142. doi:10.1007/BF00026299

Cooke, J. 2020. IUCN Red List of Threatened Species: Eubalaena glacialis. IUCN Red List of Threatened Species.

Cripps, G., P. Lindeque, and K. J. Flynn. 2014. Have we been underestimating the effects of ocean acidification in zooplankton? Global Change Biology **20**: 3377–3385. doi:10.1111/gcb.12582

Davies, K. T. A., and S. W. Brillant. 2019. Mass human-caused mortality spurs federal action to protect endangered North Atlantic right whales in Canada. Marine Policy **104**: 157–162. doi:10.1016/j.marpol.2019.02.019

Davis, G. E., M. F. Baumgartner, J. M. Bonnell, and others. 2017. Long-term passive acoustic recordings track the changing distribution of North Atlantic right whales (Eubalaena glacialis) from 2004 to 2014. Sci Rep **7**: 13460. doi:10.1038/s41598-017-13359-3

Davis, G. E., M. F. Baumgartner, P. J. Corkeron, and others. 2020. Exploring movement patterns and changing distributions of baleen whales in the western North Atlantic using a decade of passive acoustic data. Glob Change Biol **26**: 4812–4840. doi:10.1111/gcb.15191

DeLorenzo Costa, A., E. G. Durbin, and C. A. Mayo. 2006. Variability in the nutritional value of the major copepods in Cape Cod Bay (Massachusetts, USA) with implications for right whales. Marine Ecology **27**: 109–123. doi:10.1111/j.1439-0485.2006.00087.x

Diaz, B. P., B. Knowles, C. T. Johns, and others. 2021. Seasonal mixed layer depth shapes phytoplankton physiology, viral production, and accumulation in the North Atlantic. Nat Commun **12**: 6634. doi:10.1038/s41467-021-26836-1

Elith, J., S. Ferrier, F. Huettmann, and J. Leathwick. 2005. The evaluation strip: A new and robust method for plotting predicted responses from species distribution models. Ecological Modelling **186**: 280–289. doi:10.1016/j.ecolmodel.2004.12.007

Elith*, J., C. H. Graham*, R. P. Anderson, and others. 2006. Novel methods improve prediction of species' distributions from occurrence data. Ecography **29**: 129–151. doi:10.1111/j.2006.0906-7590.04596.x

Elith, J., J. R. Leathwick, and T. Hastie. 2008. A working guide to boosted regression trees. Journal of Animal Ecology **77**: 802–813. doi:10.1111/j.1365-2656.2008.01390.x

Fielding, A. H., and J. F. Bell. 1997. A review of methods for the assessment of prediction errors in conservation presence/absence models. Envir. Conserv. **24**: 38–49. doi:10.1017/S0376892997000088

Friedland, K. D., T. Miles, A. G. Goode, E. N. Powell, and D. C. Brady. 2022. The Middle Atlantic Bight Cold Pool is warming and shrinking: Indices from in situ autumn seafloor temperatures. Fisheries Oceanography **31**: 217–223. doi:10.1111/fog.12573

Gavrilchuk, K., V. Lesage, S. Fortune, and A. W. Trites. A mechanistic approach to predicting suitable foraging habitat for reproductively mature North Atlantic right whales in the Gulf of St. Lawrence.

Gonçalves Neto, A., J. Langan, and J. Palter. 2021. Changes in the Gulf Stream preceded rapid warming of the Northwest Atlantic Shelf. Communications Earth & Environment **2**. doi:10.1038/s43247-021-00143-5

Greenwell, B., M., and B. Boehmke C. 2020. Variable Importance Plots—An Introduction to the vip Package. The R Journal **12**: 343. doi:10.32614/RJ-2020-013

Grieve, B. D., J. A. Hare, and V. S. Saba. 2017. Projecting the effects of climate change on Calanus finmarchicus distribution within the U.S. Northeast Continental Shelf. Sci Rep **7**: 6264. doi:10.1038/s41598-017-06524-1

Head, E. J. H., and P. Pepin. 2010. Spatial and inter-decadal variability in plankton abundance and composition in the Northwest Atlantic (1958–2006). Journal of Plankton Research **32**: 1633–1648. doi:10.1093/plankt/fbq090

Head, E. J., L. R. Harris, and B. Petrie. 1999. Distribution of Calanus spp. on and around the Nova Scotia Shelf in April: evidence for an offshore source of Calanus finmarchicus to the central and western regions. Can. J. Fish. Aquat. Sci. **56**: 2463–2476. doi:10.1139/f99-193

Herman, A. W., D. D. Sameoto, C. Shunnian, M. R. Mitchell, B. Petrie, and N. Cochrane. 1991. Sources of zooplankton on the Nova Scotia shelf and their aggregations within deep-shelf basins. Continental Shelf Research **11**: 211–238. doi:10.1016/0278-4343(91)90066-F

Hinder, S. L., M. B. Gravenor, M. Edwards, C. Ostle, O. G. Bodger, P. L. M. Lee, A. W. Walne, and G. C. Hays. 2014. Multi-decadal range changes vs. thermal adaptation for north east Atlantic oceanic copepods in the face of climate change. Glob Change Biol **20**: 140–146. doi:10.1111/gcb.12387

Ji, R. 2011. Calanus finmarchicus diapause initiation: new view from traditional life history-based model. Marine Ecology Progress Series **440**: 105–114. doi:10.3354/meps09342

Jiménez-Valverde, A. 2012. Insights into the area under the receiver operating characteristic curve (AUC) as a discrimination measure in species distribution modelling. Global Ecology and Biogeography **21**: 498–507. doi:10.1111/j.1466-8238.2011.00683.x

Johnson, C., E. Devred, B. Casault, E. Head, and J. Spry. Optical, Chemical, and Biological Oceanographic Conditions on the Scotian Shelf and in the Eastern Gulf of Maine in 2016.

Kane, J. 2007. Zooplankton abundance trends on Georges Bank, 1977–2004. ICES Journal of Marine Science **64**: 909–919. doi:10.1093/icesjms/fsm066

Kenney, R. D., and K. F. Wishner. 1995. The South Channel Ocean Productivity EXperiment. Continental Shelf Research **15**: 373–384. doi:10.1016/0278-4343(94)00070-4

Knowlton, A. R., S. D. Kraus, and R. D. Kenney. 1994. Reproduction in North Atlantic right whales (Eubalaena glacialis). Can. J. Zool. **72**: 1297–1305. doi:10.1139/z94-173

Kraus, S. D., R. D. Kenney, C. A. Mayo, W. A. McLellan, M. J. Moore, and D. P. Nowacek. 2016. Recent Scientific Publications Cast Doubt on North Atlantic Right Whale Future. Frontiers in Marine Science **3**.

Kraus, S. D., and R. M. Rolland, eds. 2010. The Urban Whale: North Atlantic Right Whales at the Crossroads, Harvard University Press.

Kvile, K. Ø., C. Ashjian, Z. Feng, J. Zhang, and R. Ji. 2018. Pushing the limit: Resilience of an Arctic copepod to environmental fluctuations. Global Change Biology **24**: 5426–5439. doi:10.1111/gcb.14419

Laist, D. W., A. R. Knowlton, and D. Pendleton. 2014. Effectiveness of mandatory vessel speed limits for protecting North Atlantic right whales. Endangered Species Research **23**: 133–147. doi:10.3354/esr00586

Lehoux, C., S. Plourde, and V. Lesage. Significance of dominant zooplankton species to the North Atlantic Right Whale potential foraging habitats in the Gulf of St. Lawrence: a bio-energetic approach. 48.

Li, X., and Y. Wang. 2013. Applying various algorithms for species distribution modelling. Integrative Zoology **8**: 124–135. doi:10.1111/1749-4877.12000

Maillet, G., D. Bélanger, G. Doyle, A. Robar, S. Fraser, J. Higdon, D. Ramsay, and P. Pepin. Optical, Chemical, and Biological oceanographic conditions on the Newfoundland and Labrador Shelf during 2016-2017.

Mayo, C. A., B. H. Letcher, and S. Scott. 2020. Zooplankton filtering efficiency of the baleen of a North Atlantic right whale, Eubalaena glacialis. J. Cetacean Res. Manage. 225–229. doi:10.47536/jcrm.vi.286

Mayo, C. A., and M. K. Marx. 1990. Surface foraging behaviour of the North Atlantic right whale, Eubalaena glacialis, and associated zooplankton characteristics. Can. J. Zool. **68**: 2214–2220. doi:10.1139/z90-308

Meyer-Gutbrod, E., C. Greene, K. Davies, and D. Johns. 2021. Ocean Regime Shift is Driving Collapse of the North Atlantic Right Whale Population. Oceanography **34**: 22–31. doi:10.5670/oceanog.2021.308

Meyer-Gutbrod, E. L., K. T. A. Davies, C. L. Johnson, and others. Redefining North Atlantic right whale habitat-use patterns under climate change. Limnology and Oceanography **n/a**. doi:10.1002/lno.12242
Michaud, J., and C. Taggart. 2007. Lipid and gross energy content of North Atlantic right whale food,Calanus finmarchicus, in the Bay of Fundy. Endang. Species Res. **3**: 77–94. doi:10.3354/esr003077
Murison, L. D., and D. E. Gaskin. 1989. The distribution of right whales and Zooplankton in the Bay of Fundy, Canada. Can. J. Zool. **67**: 1411–1420. doi:10.1139/z89-200
Pace, R., T. Cole, and A. Henry. 2014. Incremental fishing gear modifications fail to significantly reduce large whale serious injury rates. Endang. Species. Res. **26**: 115–126. doi:10.3354/esr00635
Pace, R. M., P. J. Corkeron, and S. D. Kraus. 2017. State–space mark–recapture estimates reveal a recent decline in abundance of North Atlantic right whales. Ecology and Evolution **7**: 8730–8741. doi:10.1002/ece3.3406
Pearce, J., and S. Ferrier. 2000. Evaluating the predictive performance of habitat models developed using logistic regression. Ecological Modelling **133**: 225–245. doi:10.1016/S0304-3800(00)00322-7
Pendleton, D., P. Sullivan, M. Brown, and others. 2012. Weekly predictions of North Atlantic right whale Eubalaena glacialis habitat reveal influence of prey abundance and seasonality of habitat preferences. Endang. Species. Res. **18**: 147–161. doi:10.3354/esr00433
Pershing, A. J., M. A. Alexander, C. M. Hernandez, and others. 2015. Slow adaptation in the face of rapid warming leads to collapse of the Gulf of Maine cod fishery. Science **350**: 809–812. doi:10.1126/science.aac9819
Pershing, A. J., and K. Stamieszkin. 2020. The North Atlantic Ecosystem, from Plankton to Whales. Annu. Rev. Mar. Sci. **12**: 339–359. doi:10.1146/annurev-marine-010419-010752
Pershing, A., N. Record, B. Monger, and others. 2009. Model-based estimates of right whale habitat use in the Gulf of Maine. Mar. Ecol. Prog. Ser. **378**: 245–257. doi:10.3354/meps07829
Pettis, H., R. I. Pace, and P. Hamilton. 2022. North Atlantic Right Whale Consortium 2021 Annual Report Card. North Atlantic Right Whale Consortium.
Plourde, S., C. Lehoux, C. L. Johnson, G. Perrin, and V. Lesage. 2019. North Atlantic right whale (Eubalaena glacialis) and its food: (I) a spatial climatology of Calanus biomass and potential foraging habitats in Canadian waters. Journal of Plankton Research **41**: 667–685. doi:10.1093/plankt/fbz024
Record, N., J. Runge, D. Pendleton, and others. 2019. Rapid Climate-Driven Circulation Changes Threaten Conservation of Endangered North Atlantic Right Whales. Oceanog **32**. doi:10.5670/oceanog.2019.201
Reygondeau, G., and G. Beaugrand. 2011. Future climate-driven shifts in distribution of Calanus finmarchicus. Global Change Biology **17**: 756–766. doi:10.1111/j.1365-2486.2010.02310.x
Richardson, D. E., J. A. Hare, W. J. Overholtz, and D. L. Johnson. 2010. Development of long-term larval indices for Atlantic herring (Clupea harengus) on the northeast US continental shelf. ICES Journal of Marine Science **67**: 617–627. doi:10.1093/icesjms/fsp276
Roman, J., and J. J. McCarthy. 2010. The Whale Pump: Marine Mammals Enhance Primary Productivity in a Coastal Basin. PLOS ONE **5**: e13255. doi:10.1371/journal.pone.0013255
Ross, C. H., D. E. Pendleton, B. Tupper, D. Brickman, M. A. Zani, C. A. Mayo, and N. R. Record. 2021. Projecting regions of North Atlantic right whale, *Eubalaena glacialis* ,

habitat suitability in the Gulf of Maine for the year 2050. Elementa: Science of the Anthropocene **9**: 00058. doi:10.1525/elementa.2020.20.00058

Ross, C., J. Runge, J. Roberts, D. Brady, B. Tupper, and N. Record. Estimating North Atlantic right whale prey based on Calanus finmarchicus thresholds. Marine Ecology Progress Series **In press**.

Sameoto, D., and A. Herman. 1990. Life cycle and distribution of Calanus finmarchicus in deep basins on the Nova Scotia shelf and seasonal changes in Calanus spp. Mar. Ecol. Prog. Ser. **66**: 225–237. doi:10.3354/meps066225

Sharp, S. M., W. A. McLellan, D. S. Rotstein, and others. 2019. Gross and histopathologic diagnoses from North Atlantic right whale Eubalaena glacialis mortalities between 2003 and 2018. Diseases of Aquatic Organisms **135**: 1–31. doi:10.3354/dao03376

Smith, C. R., and A. R. Baco. ECOLOGY OF WHALE FALLS AT THE DEEP-SEA FLOOR. 44.

Sorochan, K. A., S. Plourde, R. Morse, P. Pepin, J. Runge, C. Thompson, and C. L. Johnson. 2019. North Atlantic right whale (Eubalaena glacialis) and its food: (II) interannual variations in biomass of Calanus spp. on western North Atlantic shelves. Journal of Plankton Research **41**: 687–708. doi:10.1093/plankt/fbz044

Therriault, J., B. Petrie, P. Pepin, and others. 1998. Proposal for a Northwest Atlantic Zonal Monitoring Program. 195. 195.

Thor, P., A. Bailey, C. Halsband, E. Guscelli, E. Gorokhova, and A. Fransson. 2016. Seawater pH Predicted for the Year 2100 Affects the Metabolic Response to Feeding in Copepodites of the Arctic Copepod Calanus glacialis. PLOS ONE **11**: e0168735. doi:10.1371/journal.pone.0168735

Van Der Hoop, J. M., M. J. Moore, S. G. Barco, and others. 2013. Assessment of Management to Mitigate Anthropogenic Effects on Large Whales. Conserv Biol **27**: 121–133. doi:10.1111/j.1523-1739.2012.01934.x

Villarino, E., G. Chust, P. Licandro, M. Butenschön, L. Ibaibarriaga, A. Larrañaga, and X. Irigoien. 2015. Modelling the future biogeography of North Atlantic zooplankton communities in response to climate change. Mar. Ecol. Prog. Ser. **531**: 121–142. doi:10.3354/meps11299

Wang, Z., D. Brickman, and B. J. W. Greenan. 2019. Characteristic evolution of the Atlantic Meridional Overturning Circulation from 1990 to 2015: An eddy-resolving ocean model study. Deep Sea Research Part I: Oceanographic Research Papers **149**: 103056. doi:10.1016/j.dsr.2019.06.002

Wilson, R. J., N. S. Banas, M. R. Heath, and D. C. Speirs. 2016. Projected impacts of 21st century climate change on diapause in Calanus finmarchicus. Global Change Biology **22**: 3332–3340. doi:10.1111/gcb.13282

Winn, H. E., C. A. Price, and P. W. Sorensen. 1986. The distributional biology of the right whale (Eubalaena glacialis) in the western North Atlantic. Reports - International Whaling Commission, Special Issue **10**: 129–138.

Wishner, K., E. Durbin, A. Durbin, M. Macaulay, H. Winn, and R. Kenney. 1988. Copepod Patches and Right Whales in the Great South Channel off New England. Bulletin of Marine Science **43**: 825–844.